Brief Communications

NMDA and $GABA_B$ (KIR) Conductances: The "Perfect Couple" for Bistability

Honi Sanders,[1]* Michiel Berends,[2]* Guy Major,[3] Mark S. Goldman,[2] and John E. Lisman[1]

[1]Department of Biology and Volen Center for Complex Systems, Brandeis University, Waltham, Massachusetts 02254, [2]Center for Neuroscience, Department of Neurobiology, Physiology, and Behavior, and Department of Ophthalmology and Visual Sciences, University of California, Davis, Davis, California 95618, and [3]School of Biosciences, Cardiff University, Cardiff CF10 3AX, United Kingdom

Networks that produce persistent firing in response to novel input patterns are thought to be important in working memory and other information storage functions. One possible mechanism for maintaining persistent firing is dendritic voltage bistability in which the depolarized state depends on the voltage dependence of the NMDA conductance at recurrent synapses. In previous models, the hyperpolarized state is dependent on voltage-independent conductances, including $GABA_A$. The interplay of these conductances leads to bistability, but its robustness is limited by the fact that the conductance ratio must be within a narrow range. The $GABA_B$ component of inhibitory transmission was not considered in previous analyses. Here, we show that the voltage dependence of the inwardly rectifying potassium (KIR) conductance activated by $GABA_B$ receptors adds substantial robustness to network simulations of bistability and the persistent firing that it underlies. The hyperpolarized state is robust because, at hyperpolarized potentials, the $GABA_B$/KIR conductance is high and the NMDA conductance is low; the depolarized state is robust because, at depolarized potentials, the NMDA conductance is high and the $GABA_B$/KIR conductance is low. Our results suggest that this complementary voltage dependence of $GABA_B$/KIR and NMDA conductances makes them a "perfect couple" for producing voltage bistability.

Introduction

Persistent neuronal firing underlies information storage in functions such as working memory, motor control, and spatial navigation (for review, see Goldman-Rakic, 1995; Durstewitz et al., 2000; Wang, 2001; Major and Tank, 2004). A proposed cellular mechanism underlying persistent activity is membrane potential bistability. Brief depolarizing stimuli can switch a bistable cell from a hyperpolarized state, in which the firing rate is low, to a depolarized state, in which the firing rate is high (Hounsgaard and Kiehn, 1989; Major et al., 2008). Such bistability has been observed in motoneurons and cortical and hippocampal pyramidal cells (Lee and Heckman, 1998; Schiller et al., 2000; Wei et al., 2001).

According to one hypothesis (Lisman et al., 1998), bistability depends on the voltage dependence of the NMDA receptor (NMDAR), a class of glutamate-activated channels. This voltage dependence results from block of the channel pore by extracellular Mg^{2+} (Nowak et al., 1984). This block is relieved by depolarization, leading to peak inward (depolarizing) current at elevated membrane potentials (Fig. 1*A*,*B*). Working memory networks based on this mechanism can store patterns of input by the selective persistent firing of the subset of cells excited by a brief stimulus. Even with identical recurrent synapses, current selectively flows into active (depolarized) cells through their NMDARs, thereby maintaining activity in these cells. Feedback inhibition through $GABA_A$Rs keeps other cells in the network from spuriously activating. In contrast to attractor network models of persistent firing that can only store previously learned patterns, networks with NMDAR-dependent bistability can store novel patterns (Durstewitz et al., 2000). Such models of NMDAR-dependent bistability have been extended to maintain graded patterns of activity (multistability) (Koulakov et al., 2002; Goldman et al., 2003). Consistent with a working memory function of NMDARs, antagonists of these channels interfere with delay period persistent firing (Shima and Tanji, 1998) and behaviorally measured working memory (Adler et al., 1998).

One limitation of this mechanism of producing bistability is that it requires a rather precise balancing of $GABA_A$ and NMDA conductances. Another limitation is that recurrent AMPA conductance must be very small (a 75:1 NMDA/AMPA conductance ratio was used by Lisman et al., 1998). Although NMDA-only ("silent") synapses exist, they are rare later in development (Kerchner and Nicoll, 2008). Here, we consider how these limitations might be overcome. Synaptic inhibition is due to $GABA_A$ and $GABA_B$ receptors, but previous models of bistability considered only the former. In this study, we examine the effects of

Received April 17, 2012; revised Sept. 28, 2012; accepted Oct. 4, 2012.

Author contributions: M.S.G. and J.E.L. designed research; H.S. and M.B. performed research; H.S. and M.B. analyzed data; H.S., M.B., G.M., M.S.G., and J.E.L. wrote the paper.

This work was supported by NINDS of the NIH under Award #R01DA027807 and NSF IGERT DGE-0549390 (J.E.L., H.S.), NIH Grant R01 MH069726, a Sloan Foundation Research Fellowship, and a UC Davis Ophthalmology Research to Prevent Blindness grant (M.S.G. and M.B.). We thank Michael Hasselmo for advice and Brandeis High-Performance Computing Cluster for cluster time. The content is solely the responsibility of the authors and does not necessarily represent the official views of any of the funding agencies.

*H.S. and M.B. contributed equally to this work.

Correspondence should be addressed to either of the following: Mark S. Goldman, Center for Neuroscience, Department of Neurobiology, Physiology, and Behavior, and Department of Ophthalmology and Visual Sciences, University of California, Davis, Davis, CA 95618, E-mail: msgoldman@ucdavis.edu; or John Lisman, Department of Biology and Volen Center for Complex Systems, Brandeis University, Waltham, MA 02254, E-mail: lisman@brandeis.edu.

DOI:10.1523/JNEUROSCI.1854-12.2013

 0270-6474/13/330424-06$15.00/0

including the $GABA_BR$, a G-protein-coupled receptor with a variety of downstream targets, including a G-protein-activated inwardly rectifying potassium (KIR) channel (GIRK) (Kohl and Paulsen, 2010). Like the NMDAR, the KIR channel has a Mg^{2+} block. However, because the channel is blocked by intracellular Mg^{2+} rather than extracellular Mg^{2+}, the block of the KIR channel is reduced as the cell hyperpolarizes (Yamada et al., 1998). As a result, the $GABA_B$/KIR conductance increases with hyperpolarization, enhancing outward (hyperpolarizing) current at hyperpolarized potentials (Fig. 1*A*,*B*). The potential utility of $GABA_B$Rs in bistability has been noted (Shoemaker, 2011), but the efficacy of their cooperation with NMDARs in network persistent activity has not been analyzed. Here, we show that cooperation of $GABA_B$/KIR and NMDA conductances greatly enhances the robustness of bistability in working memory networks.

Materials and Methods

Network architecture. The networks used in this study contained $N = 400$ neurons, of which $N_p = 320$ were excitatory and $N_I = 80$ were inhibitory. There were 320 incoming axons, each of which synapsed onto one excitatory cell and all inhibitory cells (feedforward inhibition was not strictly necessary, as successful simulations were run without it). The axons representing the pattern to be remembered fired a train of action potentials that was generated by a Poisson process of mean rate 200 Hz for the first 100 ms. Otherwise, incoming axons did not fire at all. The size of the activated population ranged from 10% to 75% of the total population. All excitatory neurons synapsed onto all other excitatory neurons with equal synaptic weights and onto all inhibitory neurons with equal synaptic weights. All inhibitory neurons synapsed onto all excitatory neurons with equal synaptic weights.

Neuron model. The model neurons used in this study were Hodgkin-Huxley-type conductance-based neurons, modified from Lisman et al. (1998). The excitatory neurons had two compartments: a dendrite with voltage V_d and a soma with voltage V_s. Separating the spike-generating conductances from the bistable synaptic compartment allows bistability to be maintained during the large somatic voltage fluctuations associated with action potential generation. The equations for the integration of voltage are as follows:

$$C_m\frac{dV_s}{dt} = -I_L - I_{Na} - I_K - g_c(V_s - V_d) - I_{noise}$$

$$C_m\frac{dV_d}{dt} = -I_L - g_c(V_d - V_s) - I_{syn,e} - I_{syn,ext} - I_{syn,i} - I_{GABA_B/KIR} - I_{noise}$$

where $C_m = 1\ \mu F/cm^2$ and $g_c = 0.1$ mS/cm^2.

The leak current $I_L = g_L(V - E_L)$, where $g_L = 0.1$ mS/cm^2, and $E_L = -80$ mV.

The spike-generating currents I_{Na} and I_K are described by the Hodgkin-Huxley formalism as in the work of Lisman et al. (1998), giving a threshold of ~ -45 mV and an action potential duration of ~ 1 ms. Inhibitory interneurons were as described by Wang and Buzsáki (1996).

The synaptic currents $I_{syn,e} = I_{NMDA} + I_{AMPA}$ and $I_{syn,i} = I_{GABA}$, where for AMPA and $GABA_A$, $I_x = g_x\sum_i s_i(V_d - E_x)$ (all maximal synaptic conductances g_x and reversal potentials E_x are in Table 1). $\frac{ds}{dt} = k_f\frac{1}{1+\exp(-V_{s_{pre}}/2)}(1-s) - k_r s$, where $k_f = 12\ ms^{-1}$ for both AMPA and $GABA_A$, $k_r = 1\ ms^{-1}$ for AMPA, and $k_r = 0.1\ ms^{-1}$ for $GABA_A$.

The NMDA current $I_{NMDA} = g_{NMDA}\sum_i s_i\frac{V_d - E_{NMDA}}{1 + 0.15\exp(-0.08(V_d - E_{NMDA}))}$, giving a half-activation voltage of -23.7 mV. The synaptic gating variable s has second-order kinetics conferred by $\frac{ds}{dt} = \alpha_s x(1-s) - \beta_s s$, where $\frac{dx}{dt} = \frac{\alpha_x}{1+\exp(-V_{pre}/2)}(1-x) - \beta_x x$, and $\alpha_x = 10$, $\beta_x = 0.5$, $\alpha_s = 0.1$, and $\beta_s = 0.01\ ms^{-1}$, giving an NMDA time to peak of ~ 10 ms and decay time constant of ~ 100 ms. α_s was changed from 1 as described by Lisman et al. (1998) to reflect the lack of saturation of the NMDA conductance with single spikes (Popescu et al., 2004).

The intrinsic and $GABA_B$-activated KIR current $I_{GABA_B/KIR} = g_{GABA_B/KIR}(0.25 + 0.75\sum_i s_i)\frac{V_d - E_{GABA_B/KIR}}{1+\exp(0.1(V_d - E_{GABA_B/KIR} + 10))}$ (see Yamada et al., 1998, p. 742). The factor of $(0.25 + 0.75\sum_i s_i)$ makes 25% of the maximal KIR conductance constitutively active and 75% activated through $GABA_BR$ activation of G-protein, the cooperative dynamics of which (Thomson and Destexhe, 1999) is given by $s = \frac{G^4}{G^4 + K_d}$ and four coupled first-order rate equations: the normalized G-protein concentration G changes as $\frac{dG}{dt} = K_3 R - K_4 G$, the fraction of active $GABA_BRs$ R changes as $\frac{dR}{dt} = K_1 T(1-R) - K_2 R$, extracellular GABA concentration T in mM changes as $\frac{dT}{dt} = -k_1 T(B_m - B) + k_{-1}B - (1/\tau_D)T$ and is incremented by 1 mM with each spike, and bound GABA transporter B changes as $\frac{dB}{dt} = k_1 T(B_m - B) - (k_{-1} + k_2)B$. $K_d = 17.83$, $K_1 = 0.18\ (mM^*ms)^{-1}$, $K_2 = 0.0096\ ms^{-1}$, $K_3 = 0.19\ ms^{-1}$, $K_4 = 0.060\ ms^{-1}$, $k_1 = 30\ (mM^*ms)^{-1}$, $k_{-1} = 0.1\ ms^{-1}$, $k_2 = 0.02\ ms^{-1}$, and the maximum binding capacity of transporter $B_m = 1$ mM. The only change from Thomson and Destexhe (1999) is that for each synapse, 1 mM GABA was released with each spike (instead of 3 mM) and decayed with a time constant $\tau_D = 10$ ms instead of diffusion being calculated by the gradient of transmitter. These equations give a latency of $GABA_B$-activated KIR current of ~ 10 ms, time to peak of ~ 50 ms, and a decay time constant of ~ 80 ms as described by Thomson and Destexhe (1999). A slow time constant for GABA removal was chosen because much of the $GABA_B$ response is mediated by extrasynaptic receptors (Kohl and Paulsen, 2010) and because the time constant for GABA decline at extracellular sites appears to be much slower than at synaptic sites. However, we found that results similar to those in Figure 2 could be obtained using properties characteristic of synaptic GABA (peak 3 mM; decay time constant 0.5 ms) if the decreased GABA lifetime was compensated for by raising interneuron firing rates through moderate increases in AMPA-mediated excitation onto inhibitory neurons. Thus, the model performance was robust across a broad range of assumptions about the dynamics of GABA diffusion and reuptake.

The external synaptic input $I_{syn,ext} = s_{input}\,g_{input}(V - E_{syn})$, where g_{input} is the maximal conductance given in Table 1 and the synaptic activation s_{input} is the fraction of that conductance that is activated. s_{input} increased by 50% of the as-yet-unactivated conductance (i.e., $0.5(1 - s_{input})$) with each spike and decayed exponentially with a time constant of 2 ms.

Noise was implemented as independent excitatory and inhibitory conductance noise *rand* drawn at each time step from a uniform distribution between $\pm 0.05/\sqrt{dt}$ mS/cm^2, where dt is in milliseconds. $I_{noise} =$

Table 1. Ranges of values of maximal synaptic conductances used in simulations

Synaptic conductance	Maximal g per synapse (mS/cm^2) Onto p-cells	Onto I-cells	Reversal potential
AMPA	$0.04/N_p$*	$0.5/N_p$*	0 mV
NMDA	$1–99.7/N_p$	$0.3/N_p$	0 mV
External input	2	$0.25/N_p$	0 mV
$GABA_A$	$0.1–3.2/N_I$	0	−70 mV
$GABA_B$/KIR	$0–102.4/N_I$	0	−90 mV

*The values of maximal AMPA conductances in the table do not apply where noted that AMPA scaled with NMDA. In simulations where AMPA scaled with NMDA, $g_{AMPA} = g_{NMDA}/2$ for pyramidal-to-pyramidal connections and $g_{AMPA} = g_{NMDA}/16$ for pyramidal-to-interneuron connections.

$rand^*(V - E_{AMPA}) + rand^*(V - E_{GABA_A})$. Noise was generated independently for each compartment of each cell.

Simulations. Simulations with the above model were run over all combinations of the following parameters: pattern sizes P were spaced linearly according to the formula $P = (0.1 + 0.05i)N$ for integers i from 0 to 13. Maximal conductances were chosen to give approximately even spacing on a logarithmic scale, as follows: $g_{NMDA} = (4/3)^i/10$ mS/cm^2, rounded to the nearest tenth, for i from 8 to 24; $g_{GABA_A} = 0.1$, 0.13, and $(4/3)^i/10$ mS/cm^2, rounded to the nearest tenth, for i from 3 to 12. $g_{GABA_B} = 0$ and $2^i/10$ mS/cm^2, for i from 0 to 10. The initial dendritic and somatic voltages for each neuron were chosen independently from a uniform distribution over the interval −80 to −60 mV.

To check the plausibility of the relative magnitudes of the $GABA_A$ and $GABA_B$ conductances used, we compared simulations of $GABA_A$ and $GABA_B$ IPSP magnitudes to data presented by Benardo (1994). Their Figures 6*D* and 7*B* show that the change in IPSP magnitude per 10 mV change in somatic membrane potential was ~2 mV for $GABA_B$ and ~1.7 mV for $GABA_A$, giving a ratio r of ~1.2. We checked whether our model neurons gave similar results for the conductance values used in Figure 2*B* (which is near the center of the parameter space giving successful simulations). To do this, we simulated the IPSP amplitudes measured at the soma for different somatic membrane potentials and found r of ~1.3, in good agreement with experimental values.

The criterion for successful maintenance of selective persistent activity was that the firing rate of the externally stimulated subset be >50 Hz during the last 50 ms of the 250 ms simulation, while the unstimulated population must have a firing rate of <10 Hz. The firing rates clustered bimodally above 90 Hz and below 5 Hz, so the precise cutoffs did not substantially affect the results.

Simulations were written in C++. Numerical integration was performed using Euler's method and $dt = 0.025$ ms. Code is available upon request.

Results

Previous work that did not consider $GABA_B$ (Lisman et al., 1998) showed analytically that the sum of NMDA and $GABA_A$ currents (Fig. 1*B*) can produce an "N-shaped" *I–V* (current–voltage) curve that crosses zero current at three voltages (Fig. 1*C*, solid curve). The crossings that have positive slope are stable: small perturbations from these voltages result in corrective current returning the voltage to its original level. As can be seen in the *I–V* curve, there are two zero crossings with this property, thus demonstrating bistability. However, the bistability is not very robust. Because the peaks and troughs of the *I–V* curve are relatively shallow, small changes in $GABA_A$ conductance can cause loss of one of the stable points. As shown in Figure 1*C*, ±5% change in $GABA_A$ is sufficient to destroy bistability. When $GABA_B$/KIR is added (Fig. 1*D*), the sharpness of the N-shaped *I–V* curve is increased so that $GABA_A$ can change over a much larger range

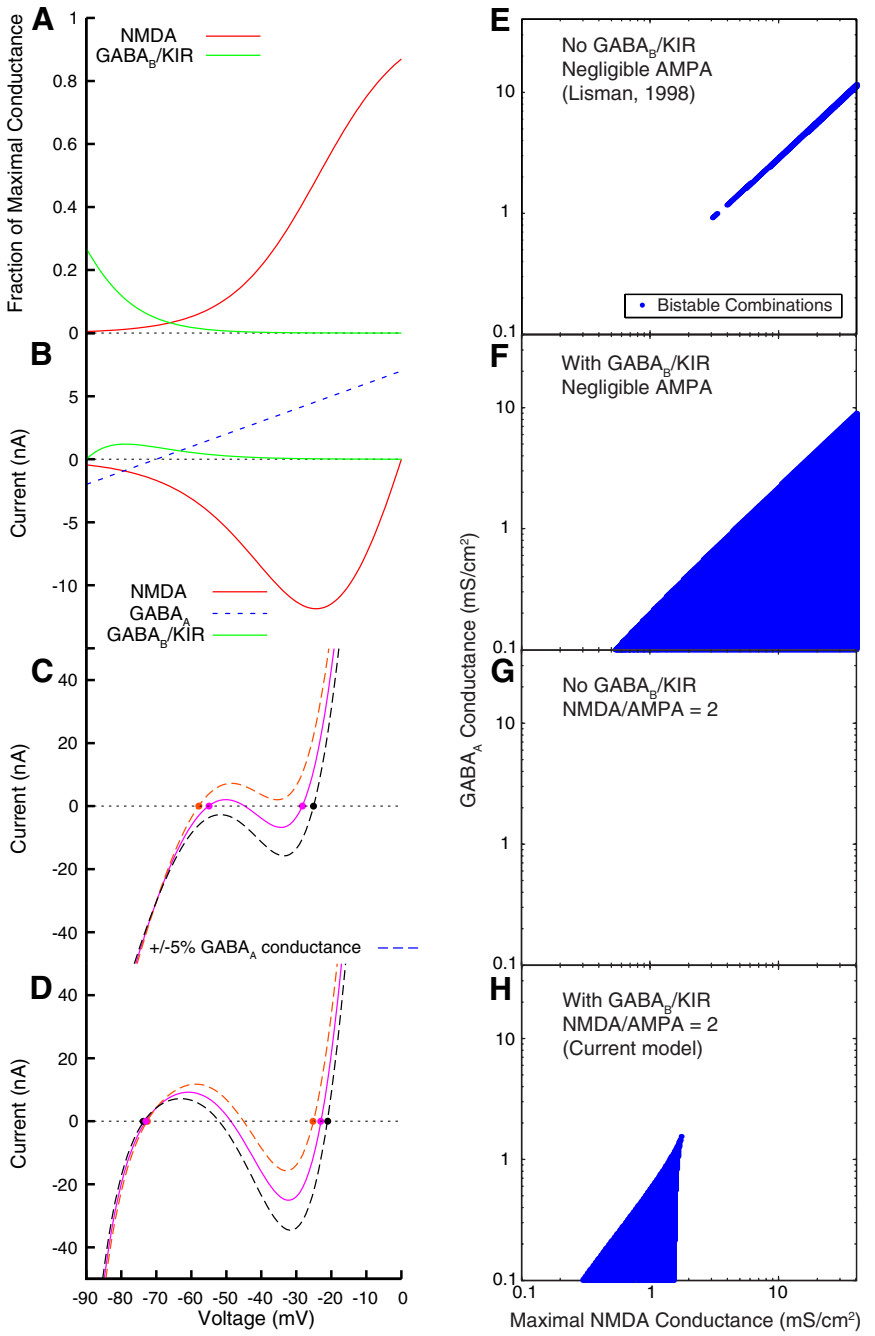

Figure 1. Voltage dependence of NMDA, $GABA_A$, and $GABA_B$/KIR currents and the robustness of the bistability that they create. ***A***, ***B***, Voltage dependence of the NMDA and $GABA_B$-activated KIR conductances (***A***) and corresponding currents $I = g(V - E_{reversal})$ for maximal conductances of 1 μS (***B***). Also shown in ***B*** is the $GABA_A$ *I–V* curve for $g_{GABA_A} = 0.1$ μS. ***C***, Combining the NMDA conductance with a $GABA_A$ conductance can produce voltage bistability. Stable points are noted by solid circles. Solid curve, *I–V* curve for 5 μS $GABA_A$ and 18 μS NMDA maximal conductances exhibits two stable membrane potentials. Dashed curves, ±5% change in $GABA_A$ conductance destroys bistability. ***D***, Adding a 40 μS $GABA_B$/KIR maximal conductance to 5 μS $GABA_A$ and 20 μS NMDA maximal conductances produces more robust bistability that is maintained through the same changes in $GABA_A$ that destroyed bistability in ***C***. ***E***, The range of combinations of $GABA_A$ and NMDA conductances that give rise to bistability without $GABA_B$ and with a fixed AMPA conductance of 0.04 mS/cm^2 (as shown by Lisman et al., 1998). ***F***, Range of bistable combinations of $GABA_A$ and NMDA is greatly expanded when a $GABA_B$/KIR conductance is added (here illustrated for a maximal $GABA_B$/KIR conductance of 51.2 mS/cm^2). ***G***, With a more typical 2:1 NMDA/AMPA ratio, there are no bistable combinations without $GABA_B$/KIR. ***H***, The $GABA_B$/KIR conductance allows bistability in dendrites with a 2:1 NMDA/AMPA maximal conductance ratio.

without loss of bistability. A more systematic exploration of the robustness produced by $GABA_B$/KIR is shown in Figure 1*E–H*. The *I–V* curve was analyzed for bistability over a wide range of combinations of $GABA_A$ and NMDA conductances. The thinness of the sliver of combinations leading to bistability in E indicates that synaptic conductances have to be precisely tuned under a model with no $GABA_B$/KIR conductance. Including a $GABA_B$/KIR conductance (Fig. 1*F*) greatly increases the range of combinations of $GABA_A$ and NMDA conductances that give bistable *I–V* curves. When the model is constrained to a more typical 2:1 NMDA/AMPA ratio (see Myme et al., 2003, their Table 1, for review), no combinations of NMDA and $GABA_A$ alone lead to bistability (Fig. 1*G*). However, when $GABA_B$/KIR is included, there is a large region of $GABA_A$ and NMDA conductance combinations that lead to bistability (Fig. 1*H*). Furthermore, the $GABA_B$/KIR conductance does not have to be precisely tuned with respect to the NMDA conductance (data not shown). Of course, if NMDA conductance is greatly decreased and/or $GABA_B$/KIR greatly increased, the dendrite will be unable to maintain the UP state, and likewise if NMDA conductance is greatly increased and/or $GABA_B$/KIR greatly decreased, the dendrite will be unable to maintain the DOWN state. However, overall, inclusion of the $GABA_B$/KIR conductance leads to robust bistability of *I–V* curves that is tolerant to large changes in either conductance.

We next examined the effects of including the $GABA_B$-activated KIR conductance in network simulations of working memory. The network (Fig. 2*A*) included 320 excitatory neurons, connected all-to-all, and 80 inhibitory interneurons that each provide global feedback inhibition. Excitatory neurons had a dendritic compartment containing the synaptic conductances connected to a somatic compartment containing the spike-generating conductances. The inhibitory neurons had a single compartment. Each excitatory neuron received external input from a single external axon; external inputs also projected non-selectively to all inhibitory neurons, although the presence of external input to inhibitory neurons was not found to be critical to the results presented below. The pattern to be stored in working memory was determined by the subset of these axons that were briefly active (200 Hz for 100 ms). KIR channels can be activated by receptors or can be constitutively active. In our simulations, 25% of the maximal KIR conductance was constitutively active and the other 75% was activated by $GABA_B$Rs through G-proteins (similar results hold for different ratios, data not shown). The relative magnitudes of $GABA_A$ and $GABA_B$/KIR conductances were chosen to be physiologically plausible (see Materials and Methods). If operating correctly, this network should selectively maintain activity in the excitatory cells that received external input. This selective maintenance should occur despite the fact that all cells receive identical recurrent presynaptic activity. As shown in Figure 2*B*, the externally activated excitatory neurons (red trace, example neuron) flip into the stable depolarized state, while excitatory neurons not receiving external input (blue trace) stably remain in the hyperpolarized state.

To understand quantitatively how persistent firing is affected by the $GABA_B$/KIR conductance, we tested the maintenance of persistent firing in the network simulation for a broad set of combinations of maximal NMDA and $GABA_A$ conductances, sizes of the input pattern to be remembered, and maximal $GABA_B$/KIR conductance (for ranges and criterion of success, see Materials and Methods).

When we ran the simulations with negligible AMPA (as described by Lisman et al., 1998), the range of acceptable conductances and pattern sizes increased dramatically when a $GABA_B$/KIR conductance was included (Fig. 2*C*,*D*, quantified in *G*). Without $GABA_B$/KIR, the range of input pattern sizes that could be selectively maintained in memory for a given combination of NMDA and $GABA_A$ conductances occupied only ~10% of the total network size. When $GABA_B$/KIR was added, the size of the input pattern could be varied over the entire range that we inspected (10%–75% of the network). We next ran simulations in which the relative AMPA component was larger (2:1 NMDA/AMPA maximal conductance ratio), as in Figure 1*G*,*H*. Under these conditions, persistent activity occurred when the $GABA_B$/KIR conductance was $>\sim 10\ mS/cm^2$ (Fig. 2*E*,*F*, quantified in *G*, left). Without $GABA_B$/KIR, none of the simulations maintained selective persistent activity. In summary, our simulations show that combining $GABA_B$/KIR with the NMDA conductance greatly enhances the robustness of bistability and persistent firing dependent on it.

Discussion

Here, we showed that the $GABA_B$-activated and intrinsic KIR conductances can work together with the NMDA conductance to produce robust bistability. In particular, we showed that bistability is maintained over much larger ranges of conductances and input pattern sizes when $GABA_B$/KIR is present than when it is not. We also showed that, with $GABA_B$/KIR, selective persistent firing can be maintained even when there is a significant AMPA component of transmission at recurrent synapses.

Networks based on the principles that we have described may be of special utility in the brain because they can store novel patterns and thus do not depend on previous learning. This stands in contrast to traditional attractor-based models of persistent firing, in which recurrent excitation is mediated by synapses whose strength has already been selectively altered by learning (Hopfield and Herz, 1995; Wang, 2001). In attractor networks, a memory trace is maintained because cells that represent a stored pattern have strong mutual synapses, while their synapses onto other cells are weak. Such networks have the disadvantage that they cannot store novel patterns. On the other hand, because they have attractor dynamics, the network can reconstruct and stably maintain patterns that are presented in a corrupted form. In our model, all synaptic weights are equal; the effective strength of connections between the neurons is determined only by the level of depolarization in the postsynaptic dendrites. This allows the network to maintain the firing of a pattern that it has never seen before, but its fidelity to the presented pattern prevents it from correcting errors. One function of such networks may be to produce the brief periods of repetitive firing that are necessary to drive attractor formation in downstream networks.

Although bistable behavior that is dependent on NMDARs has been observed in brain slices (Schiller et al., 2000; Wei et al., 2001), we predict that it is more common *in vivo*. This is because interneurons *in vivo* are typically more active than in slice preparations, leading to enhanced $GABA_B$ activation. Thus, if the bistability based on $GABA_B$ is to be investigated in slices, methods will have to be developed to activate these receptors in a manner similar to that expected *in vivo* (Kohl and Paulsen, 2010).

The NMDA and $GABA_B$/KIR conductances appear to be the perfect couple for producing bistability. Most notably, the two conductances have a complementary voltage dependence: in the depolarized state, the NMDA conductance is "on," whereas the KIR channel activated by $GABA_B$ is "off"; the converse is true in the hyperpolarized state. Furthermore, bistability requires that the conductance ratio of $GABA_B$/KIR to NMDA stays within a

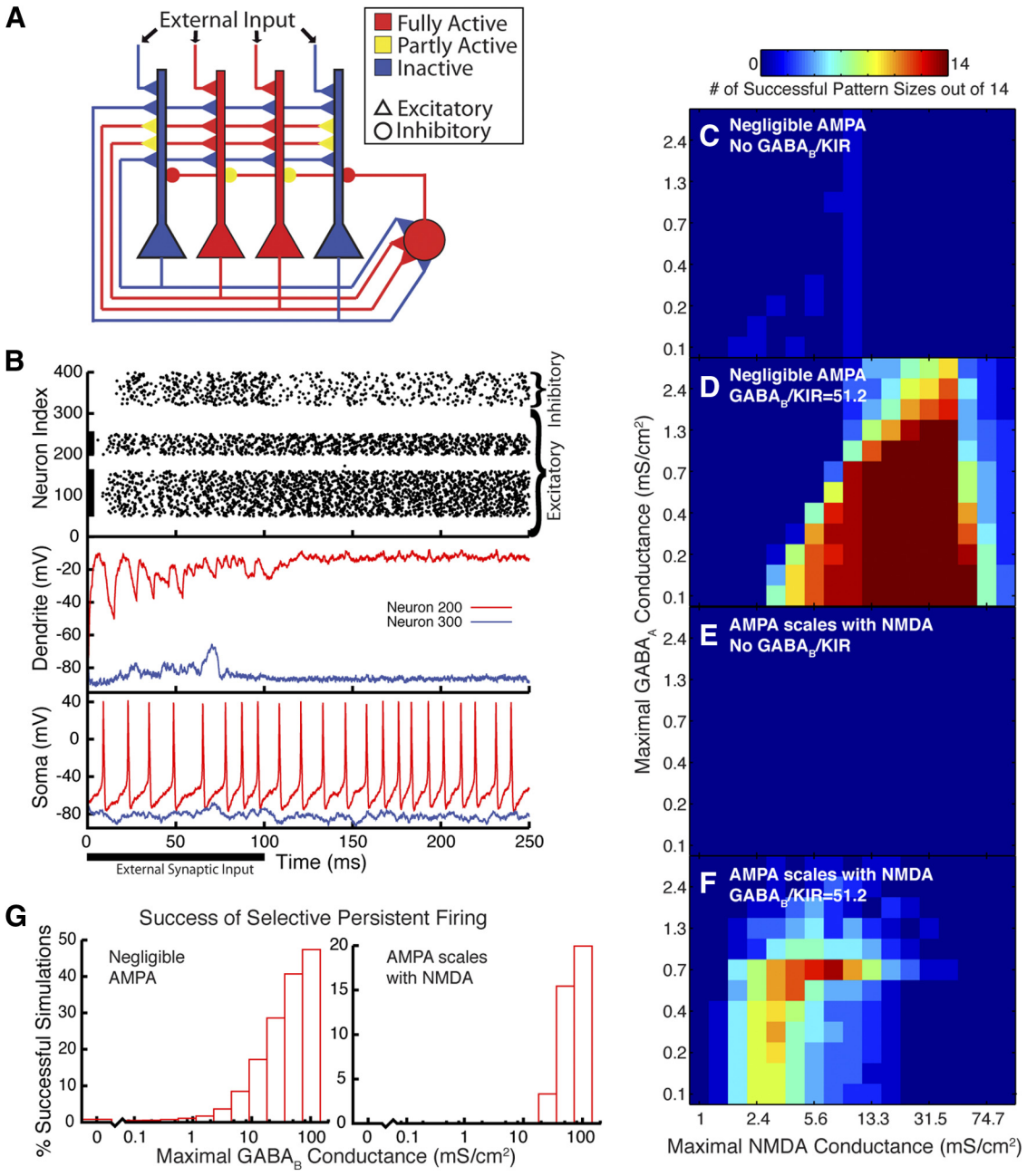

Figure 2. Robustness of persistent firing in network simulations is increased by including $GABA_B$/KIR. ***A***, Network architecture. A subset of excitatory cells (large triangular somas with rectangular dendrites) receive external synaptic input for 100 ms. The dendrites of these cells are depolarized (red), leading to somatic firing (red), while the dendrites of the other cells are hyperpolarized (blue). Recurrent excitatory axons cause both NMDA and AMPA current to pass at their synapses onto depolarized dendrites (small red triangles), while little NMDA current passes at synapses onto hyperpolarized dendrites (yellow). Inhibitory axons cause both $GABA_A$ and $GABA_B$/KIR current to pass at their synapses onto hyperpolarized dendrites (small red circles), while little $GABA_B$/KIR current passes at synapses onto depolarized dendrites (yellow). ***B***, Top, Initially stimulated cells (black bars on *y*-axis) maintain their firing after external stimulation ends, without activity spreading to other cells (black points at time of each spike). Bottom, Neuron 200, which is in the activated subset, continues to fire after the external input ceases, while neuron 300 barely moves away from its resting potential despite receiving the same presynaptic activation as neuron 200 after the first 100 ms. Maximal conductances: NMDA, 7; AMPA, 3.5; $GABA_B$/KIR, 50; $GABA_A$, 0.7 mS/cm^2; 160 excitatory cells initially stimulated. The voltage dependence of the $GABA_B$/KIR conductance causes the very large nominal $GABA_B$/KIR to $GABA_A$ conductance ratio despite their reasonable effective conductance ratio (see Materials and Methods). ***C–G***, The simulation was run repeatedly, varying the size of the initially stimulated population and maximal $GABA_A$, $GABA_B$/KIR, and NMDA conductances (see Materials and Methods). The number of successful pattern sizes of 14 tested pattern sizes for a given combination of conductances is shown. ***C***, Combinations of maximal $GABA_A$ and NMDA conductances that lead to selective persistent activity for simulations based on the original model (Lisman et al., 1998) (no $GABA_B$/KIR, negligible AMPA). ***D***, Adding the $GABA_B$/KIR conductance increases the robustness of the persistent firing. ***E***, If the NMDA/AMPA maximal conductance ratio was set at a more typical value of 2, no simulations produced selective persistent activity without $GABA_B$/KIR. ***F***, With the addition of sufficient $GABA_B$/KIR conductance, selective persistent activity did occur. ***G***, The proportion of simulations over the tested range of parameters that exhibited selective persistent activity increases with the addition of the $GABA_B$/KIR conductance. Each bar represents an average over an entire 2-D plot of the type illustrated in ***C–F***. For example, ***C*** is quantified in the leftmost bar of the left bar graph and ***F*** is quantified in the penultimate bar of the right bar graph.

certain range. The fact that both conductances have long time constants of decay helps to smooth out fluctuations and thereby maintain a fixed ratio. Another way in which they are well suited for balancing each other is that both conductances scale with network activity. This enhances robustness compared with the situation in which NMDA current scales with activity, but the KIR conductance is fixed (Gruber et al., 2003). Some limits on perfect balancing of the two conductances should, however, be noted. Constitutively active KIR (Doupnik et al., 1995) or KIR channels activated by neuromodulators (Yamada et al., 1998) may also be beneficial for maintaining persistent firing, for example by providing a baseline level of KIR current while additional $GABA_B$/KIR conductance slowly activates. This means that the activity-dependent scaling of NMDA and $GABA_B$/KIR will not be exact. Furthermore, it is unclear exactly how well the time course of the two conductances match, as the time course of $GABA_B$ can vary widely over brain regions (Thomson and Destexhe, 1999); measurement of the two conductances under the same conditions would be useful for more detailed analysis of this issue.

It had generally been assumed that the functions of $GABA_B$ were based on its slow time course (e.g., theta oscillations; Wallenstein and Hasselmo, 1997). Our work suggests that the strong voltage dependence of the $GABA_B$/KIR conductance is also important, specifically that this voltage dependence couples with that of the NMDA conductance to produce a robust form of membrane voltage bistability. Such bistability may be important in various forms of working memory. Previous work has shown that NMDAR antagonists interfere with working memory (Adler et al., 1998). It will thus be important to test whether $GABA_B$ antagonists or interneuron hypofunction also produce deficits in working memory. With this in mind, the $GABA_B$/KIR conductance should be taken into account in further work on bistability and working memory.

References

Adler CM, Goldberg TE, Malhotra AK, Pickar D, Breier A (1998) Effects of ketamine on thought disorder, working memory, and semantic memory in healthy volunteers. Biol Psychiatry 43:811–816. CrossRef Medline

Benardo L (1994) Separate activation of fast and slow inhibitory postsynaptic potentials in rat neocortex in vitro. J Physiol 203–215.

Doupnik CA, Davidson N, Lester HA (1995) The inward rectifier potassium channel family. Curr Opin Neurobiol 5:268–277. CrossRef Medline

Durstewitz D, Seamans J, Sejnowski T (2000) Neurocomputational models of working memory. Nat Neurosci 3 [Suppl]:1184–1191.

Goldman MS, Levine JH, Major G, Tank DW, Seung HS (2003) Robust persistent neural activity in a model integrator with multiple hysteretic dendrites per neuron. Cereb Cortex 13:1185–1195. CrossRef Medline

Goldman-Rakic PS (1995) Cellular basis of working memory. Neuron 14: 477–485. CrossRef Medline

Gruber AJ, Solla SA, Surmeier DJ, Houk JC (2003) Modulation of striatal single units by expected reward: a spiny neuron model displaying dopamine-induced bistability. J Neurophysiol 90:1095–1114. CrossRef Medline

Hopfield JJ, Herz AV (1995) Rapid local synchronization of action potentials: toward computation with coupled integrate-and-fire neurons. Proc Natl Acad Sci U S A 92:6655–6662. CrossRef Medline

Hounsgaard J, Kiehn O (1989) Serotonin-induced bistability of turtle motoneurones caused by a nifedipine-sensitive calcium plateau potential. J Physiol 414:265–282. Medline

Kerchner GA, Nicoll RA (2008) Silent synapses and the emergence of a postsynaptic mechanism for LTP. Nat Rev Neurosci 9:813–825. CrossRef Medline

Kohl MM, Paulsen O (2010) The roles of GABAB receptors in cortical network activity. Adv Pharmacol 58:205–229. CrossRef Medline

Koulakov AA, Raghavachari S, Kepecs A, Lisman JE (2002) Model for a robust neural integrator. Nat Neurosci 5:775–782. CrossRef Medline

Lee RH, Heckman CJ (1998) Bistability in spinal motoneurons in vivo: systematic variations in rhythmic firing patterns. J Neurophysiol 80: 572–582. Medline

Lisman JE, Fellous JM, Wang XJ (1998) A role for NMDA-receptor channels in working memory. Nat Neurosci 1:273–275. CrossRef Medline

Major G, Tank D (2004) Persistent neural activity: prevalence and mechanisms. Curr Opin Neurobiol 14:675–684. CrossRef Medline

Major G, Polsky A, Denk W, Schiller J, Tank DW (2008) Spatiotemporally graded NMDA spike/plateau potentials in basal dendrites of neocortical pyramidal neurons. J Neurophysiol 99:2584–2601. CrossRef Medline

Myme CI, Sugino K, Turrigiano GG, Nelson SB (2003) The NMDA-to-AMPA ratio at synapses onto layer 2/3 pyramidal neurons is conserved across prefrontal and visual cortices. J Neurophysiol 90:771–779. CrossRef Medline

Nowak L, Bregestovski P, Ascher P, Herbet A, Prochiantz A (1984) Magnesium gates glutamate-activated channels in mouse central neurones. Nature 307:462–465. CrossRef Medline

Popescu G, Robert A, Howe JR, Auerbach A (2004) Reaction mechanism determines NMDA receptor response to repetitive stimulation. Nature 430:790–793. CrossRef Medline

Schiller J, Major G, Koester HJ, Schiller Y (2000) NMDA spikes in basal dendrites of cortical pyramidal neurons. Nature 404:285–289. CrossRef Medline

Shima K, Tanji J (1998) Involvement of NMDA and non-NMDA receptors in the neuronal responses of the primary motor cortex to input from the supplementary motor area and somatosensory cortex: studies of task-performing monkeys. Jpn J Physiol 48:275–290. CrossRef Medline

Shoemaker PA (2011) Neural bistability and amplification mediated by NMDA receptors: analysis of stationary equations. Neurocomputing 74: 3058–3071. CrossRef

Thomson AM, Destexhe A (1999) Dual intracellular recordings and computational models of slow inhibitory postsynaptic potentials in rat neocortical and hippocampal slices. Neuroscience 92:1193–1215. CrossRef Medline

Wallenstein GV, Hasselmo ME (1997) GABAergic modulation of hippocampal population activity: sequence learning, place field development, and the phase precession effect. J Neurophysiol 78:393–408. Medline

Wang XJ (2001) Synaptic reverberation underlying mnemonic persistent activity. Trends Neuroci 24:455–463. CrossRef

Wang XJ, Buzsáki G (1996) Gamma oscillation by synaptic inhibition in a hippocampal interneuronal network model. J Neurosci 16:6402–6413. Medline

Wei DS, Mei YA, Bagal A, Kao JP, Thompson SM, Tang CM (2001) Compartmentalized and binary behavior of terminal dendrites in hippocampal pyramidal neurons. Science 293:2272–2275. CrossRef Medline

Yamada M, Inanobe A, Kurachi Y (1998) G protein regulation of potassium ion channels. Pharmacol Rev 50:723–760. Medline